Arabidopsis ABCG28 is required for the apical accumulation of reactive oxygen species in growing pollen tubes

Thanh Ha Thi Do[a], Hyunju Choi[a], Michael Palmgren[b], Enrico Martinoia[a,c], Jae-Ung Hwang[a], and Youngsook Lee[a,1]

[a]Division of Integrative Bioscience and Biotechnology, POSTECH, 37673 Pohang, Republic of Korea; [b]Department of Plant and Environmental Sciences, University of Copenhagen, DK-1871 Frederiksberg, Denmark; and [c]Department of Plant and Microbial Biology, University of Zurich, 8008 Zurich, Switzerland

Edited by Julian I. Schroeder, University of California, San Diego, La Jolla, CA, and approved May 6, 2019 (received for review February 11, 2019)

Tip-focused accumulation of reactive oxygen species (ROS) is tightly associated with pollen tube growth and is thus critical for fertilization. However, it is unclear how tip-growing cells establish such specific ROS localization. Polyamines have been proposed to function in tip growth as precursors of the ROS, hydrogen peroxide. The ABC transporter AtABCG28 may regulate ROS status, as it contains multiple cysteine residues, a characteristic of proteins involved in ROS homeostasis. In this study, we found that *AtABCG28* was specifically expressed in the mature pollen grains and pollen tubes. AtABCG28 was localized to secretory vesicles inside the pollen tube that moved toward and fused with the plasma membrane of the pollen tube tip. Knocking out *AtABCG28* resulted in defective pollen tube growth, failure to localize polyamine and ROS to the growing pollen tube tip, and complete male sterility, whereas ectopic expression of this gene in root hair could recover ROS accumulation at the tip and improved the growth under high-pH conditions, which normally prevent ROS accumulation and tip growth. Together, these data suggest that AtABCG28 is critical for localizing polyamine and ROS at the growing tip. In addition, this function of AtABCG28 is likely to protect the pollen tube from the cytotoxicity of polyamine and contribute to the delivery of polyamine to the growing tip for incorporation into the expanding cell wall.

pollen tube growth | ROS | polyamine | ABC transporters | AtABCG28

Reactive oxygen species (ROS), including hydrogen peroxide (H_2O_2), superoxide (O_2^-), and hydroxyl radical (OH·), are inevitable by-products of aerobic life (1). Of these by-products, hydrogen peroxide is stable and can function as a signaling molecule (2). Tip-focused ROS accumulation is important for directional growth, such as that observed in pollen tubes and root hairs, filamentous fungi, fucoid brown algae, and migrating animal cells such as embryonic cells and leukocytes (3–6). Tip-focused ROS accumulation, particularly of hydrogen peroxide, can activate downstream targets, which in turn activate directional growth (7, 8). An unresolved question is how hydrogen peroxide accumulates specifically at the tip, despite its chemical properties which should allow rapid diffusion in the cytosol (9). In migrating animal cells, tip-focused ROS accumulation was proposed to be established through the specific subcellular localization of NADPH oxidase, which catalyzes the production of superoxide (10). In plants, a similar mechanism has been demonstrated to exist in root hairs; *AtRBOHC*, an *Arabidopsis thaliana* homolog of $gp91^{phox}$, the glycosylated transmembrane subunit of the mammalian NADPH oxidase cytochrome, contributes to the generation of tip-focused ROS (11, 12). However, in pollen tubes, a similar mechanism does not sufficiently explain how tip-focused ROS accumulation is established (discussed below).

Two sources of ROS generation have been reported in the pollen tube: NADPH oxidases, which produce superoxide from NADPH (13), and polyamine oxidase (PAO), which uses polyamines as substrate to produce hydrogen peroxide (14). Two NADPH oxidases that are highly expressed in mature pollen grains and are localized to the plasma membrane in the pollen tube tip have been reported to catalyze the production of ROS (15, 16). According to the current hypothesis, NADPH oxidases produce superoxide at the apoplastic side of the apex of the growing tip, which is then converted to hydrogen peroxide by the activity of the superoxide dismutase in the apoplast (17). Hydrogen peroxide thus produced diffuses to the pollen tube tip, probably via aquaporins, where it accumulates, forming a tip-focused distribution of ROS (18). However, double-knockout plants lacking both NADPH oxidases can produce pollen tubes that elongate normally until the late stages of pollen tube growth, whereas tip-focused accumulation of ROS seems to be required for pollen tube elongation from emergence (19, 20).

Polyamines are a group of amines (such as putrescine, spermidine, and spermine) that exist in almost all living organisms (21, 22). Multiple lines of evidence indicate that spermine and spermidine contribute directly to ROS generation in pollen tubes and pollen tube growth. First, pollen tubes express high levels of polyamine biosynthesis genes during the first 30 min of growth (23), and polyamines have been detected in germinating and elongating pollen tubes (24). Second, genes encoding PAOs, which generate hydrogen peroxide by oxidizing polyamines, are expressed in elongating pollen tubes (25); *AtPAO3* is expressed in pollen tubes and generates ROS during pollen tube growth in the presence of exogenous spermidine (14). Third, FITC-conjugated spermine localizes to the pollen tube tip in a pattern similar to that reported for ROS (26). Fourth, pollen fail to germinate when polyamine synthesis is inhibited (27). Fifth, exogenously applied spermine alters the cell wall deposition pattern at

Significance

Reactive oxygen species (ROS) are observed at the growing site of directional cell growth in many organisms, including the tip-growing pollen tubes. This work identifies an ABC transporter, AtABCG28, as a critical factor for ROS accumulation at the tip of the growing *Arabidopsis thaliana* pollen tube. This function of AtABCG28 is due to its involvement in accumulating secretory vesicles containing polyamines, precursors of ROS, to the growing tip. Thus, this study provides a mechanism underlying the spatial organization of ROS in a single cell, which is mediated by a transporter.

Author contributions: T.H.T.D., H.C., J.-U.H., and Y.L. designed research; T.H.T.D. performed research; H.C. isolated knockout mutants; T.H.T.D. analyzed data; and T.H.T.D., M.P., E.M., J.-U.H., and Y.L. wrote the paper.

The authors declare no conflict of interest.

This article is a PNAS Direct Submission.

[1]To whom correspondence may be addressed. Email: ylee@postech.ac.kr.

This article contains supporting information online at www.pnas.org/lookup/suppl/doi:10.1073/pnas.1902010116/-/DCSupplemental.

Published online May 31, 2019.

the tip of pollen tubes (28). Finally, spermidine stimulates the elongation of pollen tubes in a defined concentration range (29).

Polyamine levels within cells must be stringently regulated; whereas polyamines are necessary for active growth, they are intrinsically toxic because, as polycations at intracellular pH (30), they bind strongly to subcellular organelles and high-molecular-weight compounds such as DNA and RNA and can interfere with their functions (31, 32). Polyamine transporters localized to multiple membrane systems control cellular polyamine homeostasis. For instance, at the plasma membrane of tip-growing cells, which require high levels of polyamines, polyamines are taken up by transporter proteins to supplement de novo polyamine synthesis (33). Furthermore, polyamine transporters have been found to localize to the membranes of intracellular organelles, such as chloroplasts, Golgi, and secretory vesicles (reviewed in ref. 33). In mammalian neuronal cells and mast cells, a member of the solute carrier transporter family, SLC18, mediates polyamine uptake into secretory vesicles (34–36). In prokaryotes and yeast, ABC (ATP-binding cassette) transporters and many other types of proteins transport polyamines (37, 38). In plants, several L-type amino acid transporters transport polyamines. Screens for mutant plants exhibiting improved tolerance to paraquat, a herbicide structurally resembling putrescine (a diamine), identified candidate transporters of polyamines at the plasma membrane and chloroplast (33, 39–41). Among them, AtLAT1 was shown to transport polyamines (33). Improved tolerance to paraquat was also observed in a mutant lacking the ABC transporter AtPDR11 (42), suggesting that AtPDR11 functions in polyamine transport. Many more polyamine transporters are likely to exist, as polyamines are involved in numerous physiological and developmental processes.

The ABC transporters are involved in various developmental processes in living organisms (43), and some of them play important roles in protecting cells from toxic molecules by removing them from the cytosol (44). In mammals, the ABC transporter HsABCG2 was suggested to transport heme, which induces ROS production under hypoxic conditions (45). Many members of the ABCG subfamily of ABC proteins participate in pollen development (46), and this subfamily includes members with multiple cysteine residues and cysteine–proline motifs that might be involved in oxidation/reduction reactions (Fig. 1). Thus, ABCG proteins are candidate polyamine transporters in pollen.

In this study, we examined whether any ABCG transporters are involved in the transport of ROS-related compounds such as polyamines. We identified the *A. thaliana* ABC transporter AtABCG28 as an essential factor for the generation of tip-focused ROS accumulation in pollen tubes during the early stages of growth, and for the successful reproduction of male gametes. Moreover, we provided experimental evidence for the role of this ABC transporter in generating the tip-focused distribution of polyamines in growing pollen tubes. We envisage two models for the mechanism of action of AtABCG28: sequestration of polyamines into intracellular secretory vesicles or trafficking of the secretory vesicles containing polyamines to the growing pollen tube tip. Such a mechanism would enable hydrogen peroxide production both inside the vesicles moving to the tip and at the apoplast after fusion of the vesicles to the plasma membrane.

Results

AtABCG28 Has a Unique Structure with Numerous Thiol Groups. Proteins involved in redox regulation and signaling often possess many thiol groups in their active center, which allow them to switch between oxidized and reduced forms (47). To identify ABCG proteins that could potentially transport ROS-related compounds, we searched for ABCG proteins with multiple thiol groups in Aramemnon, a database of plant membrane proteins (48). We found that AtABCG24, AtABCG28, and AtNAP12 contain

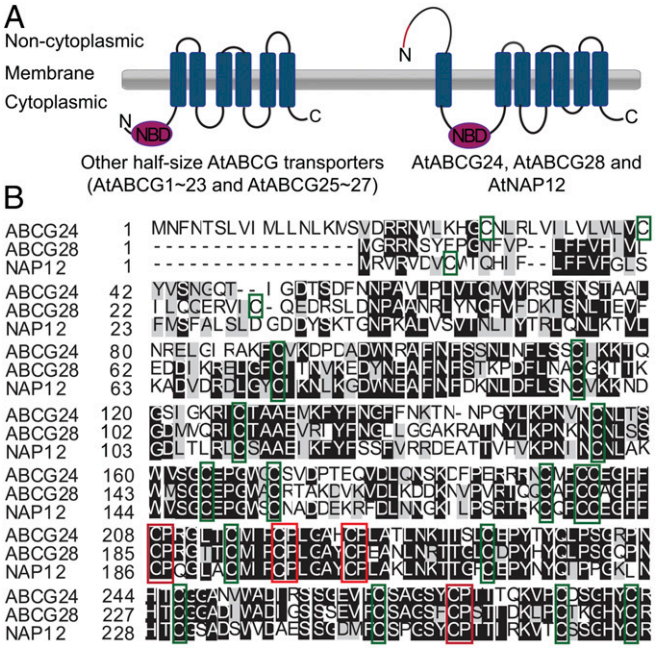

Fig. 1. The predicted topology of the three ABCG transporters that contain many cysteine residues is different from that of other half-size ABCG transporters in *A. thaliana*. (*A*) Predicted topology of the three half-size ABCG transporters containing many cysteine residues (AtABCG24, AtABCG28, and AtNAP12; *Right*) and that of other half-size ABCG transporters (*Left*). Topology and domain organization are based on the Aramemnon database (http://aramemnon.uni-koeln.de) and SPOCTOPUS program (http://octopus.cbr.su.se/). AtABCG24, AtABCG28, and AtNAP12 are predicted to have an extra non-cytoplasmic domain at the N terminus compared with other half-size ABCG transporters. The red line in the N terminus indicates the predicted signal peptide. (*B*) AtABCG24, AtABCG28, and AtNAP12 contain numerous thiol groups in the predicted N-terminal noncytoplasmic domains. The cysteine residues with thiol groups are boxed in green, and the cysteine–proline motifs, which are known as heme regulatory motifs, are boxed in red.

~37 cysteine residues. Furthermore, these ABCG transporters are predicted to have a unique topology that differs from that of the other members of the half-size ABCG subfamily; they have a long extracellular domain (consisting of ~200 amino acid residues) at the N terminus (Fig. 1*A*), where ~23 cysteine residues are located (Fig. 1*B*).

We focused our study on *AtABCG28* (At5g60740) and *AtNAP12* (At2g37010), since they are highly expressed in mature pollen grains (*SI Appendix*, Fig. S1). If either of these ABC proteins plays a critical role in ROS generation in the pollen, the corresponding knockout plants are likely to have defects in pollen germination and pollen tube growth, and hence reduced fertility. Thus, we isolated their knockout mutants and assayed their reproductive competence.

The Male Gametophyte of *atabcg28* T-DNA Insertion Mutants Is Sterile. T-DNA insertion mutant seeds harboring defects in *AtNAP12* and *AtABCG28* were obtained from SALK and SAIL and from GABI-KAT, respectively (*SI Appendix*, Fig. S2). We isolated two independent homozygous *atnap12* knockouts (*SI Appendix*, Fig. S2 *A–C*) but were unable to isolate homozygous mutants for the two *atabcg28* alleles (Table 1 and *SI Appendix*, Fig. S2 *D–F*). The dramatic phenotype of *atabcg28* suggested that AtABCG28 functions in fertilization, and we thus decided to examine this gene further.

Self-fertilized *atabcg28*/+ mutants produced wild-type ($^{+/+}$) and *atabcg28*/+ progeny at a 1:1 ratio, revealing that either the male or female gametophyte carrying the *atabcg28* mutation is

Table 1. Disruption of AtABCG28 resulted in gametophytic defects

Parent	F1					
	Sul^S ($^{+/+}$)	Sul^R (*atabcg28*$^{-/+}$ and *atabcg28*$^{-/-}$)	*n*	Ratio	χ^2	*P* value
atabcg28-1$^{-/+}$	1,187	1,156	2,343	1.0:1.0	30.720	<0.0001
atabcg28-2$^{-/+}$	949	1,052	2,001	1.0:1.1	41.813	<0.0001
atabcg28-1$^{-/+}$; *pAtABCG28:gAtABCG28*$^{-/+}$						
Line 2	38	79	117	1.0:2.1	2.613	>0.05, ns
Line 5	36	85	121	1.0:2.4	1.333	>0.05, ns
Line 6	28	90	118	1.0:3.2	0.053	>0.05, ns
Line 9	35	74	109	1.0:2.1	2.613	>0.05, ns
Line 12	32	86	118	1.0:2.7	0.213	>0.05, ns
atabcg28-2$^{-/+}$; *pAtABCG28:gAtABCG28*$^{-/+}$						
Line 8	29	58	87	1.0:2.0	3.413	>0.05, ns
Line 15	36	84	120	1.0:2.3	1.333	>0.05, ns
Line 17	17	46	63	1.0:2.7	0.213	>0.05, ns
Line 18	19	42	61	1.0:2.2	1.920	>0.05, ns
Line 19	17	40	57	1.0:2.4	1.333	>0.05, ns

The self-fertilized progeny of two independent alleles of atabcg28$^{-/+}$ plants segregated at a ratio of 1:1 instead of 1:3 (Mendelian inheritance); complementation with a genomic fragment of AtABCG28 (pAtABCG28:gAtABCG28) restored the ratio to ~1:3. Genotypes of progeny were determined based on resistance to sulfadiazine. *P* values were calculated using a χ^2 test, with a ratio of Sul^S:Sul^R = 1:3 expected for Mendelian inheritance. Sul^R, sulfadiazine resistant; Sul^S, sulfadiazine sensitive. ns, not significantly different from the 1:3 ratio of Mendelian inheritance.

defective (Table 1). Analyses of reciprocal crosses of *atabcg28*/+ and the wild type revealed that male gametophytes carrying a mutation in *atabcg28* were sterile. When *atabcg28*/+ was used as the pollen donor, we obtained only wild-type progeny, and no *atabcg28*/+ mutants (Table 2). However, when *atabcg28*/+ was the pollen acceptor, we obtained both *atabcg28*/+ heterozygous and wild-type progeny at a 1:1 ratio, which indicated that the *atabcg28* female gametophyte produced progeny as successfully as the wild type. Introducing a genomic fragment of *AtABCG28* (*gAtABCG28*) (*SI Appendix*, Fig. S3*A*) fully complemented the fertility defect of *atabcg28*/+ mutants (Table 1). The results indicated that *AtABCG28* was important for the reproductive success of the male gamete.

***AtABCG28* Is Expressed Specifically in Mature Pollen Grains and in Pollen Tubes.** We next examined the tissue-specific and developmental stage-specific expression patterns of *AtABCG28* using transgenic *A. thaliana* plants expressing a GUS reporter driven by the *AtABCG28* promoter (*pAtABCG28*::GUS in *SI Appendix*, Fig. S3*B*). The GUS signal was detectable in mature flowers (Fig. 2*A*), particularly in mature pollen grains and in pollen tubes (Fig. 2*B*), but not in other tissues of the plant. The expression pattern was consistent with that reported in a transcriptomic database (ref. 49 and *SI Appendix*, Fig. S1) and with the male gametophyte-specific defect of the *atabcg28*/+ mutant plant (Table 2).

AtABCG28 Is Localized to Secretory Vesicles at the Tips of Growing Pollen Tubes. To determine the subcellular localization of AtABCG28, we stably expressed *mGFP4:gAtABCG28* driven by its endogenous promoter (*pAtABCG28*::*mGFP4:gAtABCG28*), in which green fluorescent protein (mGFP4) was fused to *gAtABCG28* downstream of the signal peptide (*SI Appendix*, Fig. S3*C*). The *pAtABCG28*::*mGFP4:gAtABCG28* construct could recover the pollen tube growth (*SI Appendix*, Fig. S4) and fertility of *atabcg28* pollen (*SI Appendix*, Table S1). The *pAtABCG28*::*mGFP4:gAtABCG28* signal appeared to concentrate at the pollen tube tip and was also transiently incorporated into the apical plasma membrane (*SI Appendix*, Fig. S5*A*). However, the fluorescence intensity was weak. Therefore, we complemented *atabcg28*/+ with *pLAT52*::*EYFP:gAtABCG28*, in which the enhanced yellow fluorescent protein (EYFP) was fused to *gAtABCG28* downstream of the signal peptide and driven by the strong pollen-specific LAT52 promoter (*SI Appendix*, Figs. S3*D* and S4 and Table S1). In growing *pLAT52*::*EYFP*:*gAtABCG28* pollen tubes, the EYFP signal was localized to small vesicles and transiently appeared at the apical plasma membrane (Fig. 2*C* and *SI Appendix*, Fig. S5*B*), similarly to *pAtABCG28*::*mGFP4:gAtABCG28* (*SI Appendix*, Fig. S5*A*). This

Table 2. Reciprocal crosses of atabcg28$^{-/+}$ and wild-type ($^{+/+}$) plants revealed that in atabcg28$^{-/+}$ the female gametophyte is normal, while the male gametophyte is completely sterile

Parent			F1					
Female		Male	Sul^S ($^{+/+}$)	Sul^R (*atabcg28*$^{-/+}$)	*n*	Ratio	χ^2	*P* value
atabcg28-1$^{-/+}$	x	$^{+/+}$	638	602	1,240	1:1	0.04	0.8415
atabcg28-2$^{-/+}$	x	$^{+/+}$	999	950	1,949	1:1	0.04	0.8415
$^{+/+}$	x	*atabcg28-1*$^{-/+}$	539	0	539	1:0	100	<0.0001
$^{+/+}$	x	*atabcg28-2*$^{-/+}$	2,142	0	2,142	1:0	100	<0.0001

When wild-type ($^{+/+}$) was pollen donor, ~50% of the F1 progeny were atabcg28$^{-/+}$, whereas when atabcg28$^{-/+}$ was pollen donor, only $^{+/+}$ F1 progeny were produced. *P* values were calculated by a χ^2 test, using an expected ratio of 1:1.

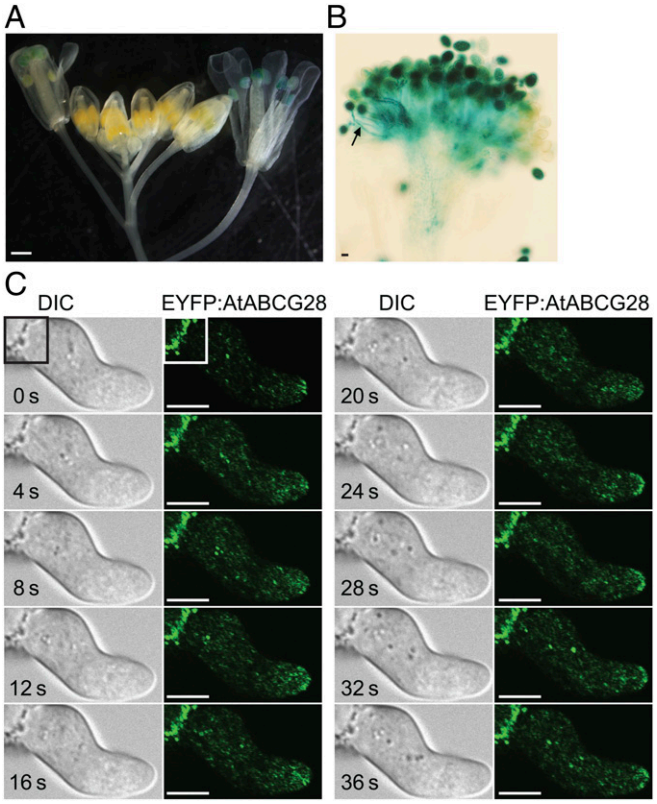

Fig. 2. AtABCG28 is expressed specifically in mature pollen grains and localizes to the secretory vesicles at the growing pollen tube tip. (*A* and *B*) Tissue-specific expression pattern of pAtABCG28::GUS in an inflorescence stem (*A*) and in a pollinated pistil (*B*). Note that the pAtABCG28::GUS signal is apparent in anthers and pollinated pistils of the flowers at stage 12–13. [Scale bars, 100 μm (*A*) and 10 μm (*B*).] (*C*) Time-lapse images of EYFP:AtABCG28 pollen in the apical zone of the tube during the initial slow-growing phase. Note that the EYFP:AtABCG28 signal appears as bright dots moving toward the growing tip and transiently accumulates in the plasma membrane at t = 12, 24, 28, and 32 s. The bright fluorescence in the left corner of the image (white rectangle) is autofluorescence from the pollen coat. (Scale bars, 5 μm.)

localization was similar to that of secretory vesicles reported previously (50). Remarkably, the intensity of the EYFP:AtABCG28 fluorescence signal at the apical plasma membrane fluctuated multiple times in growing pollen tubes (Fig. 2*C* and *SI Appendix*, Fig. S5). We suspected that the EYFP:AtABCG28 belongs to secretory vesicles. To test this possibility, we treated the pollen tubes with brefeldin A (BFA), which has been shown to inhibit vesicular secretion in pollen tubes (51, 52) by inhibiting GNOM ARF-GEF, an essential regulator of protein secretion (53). We then observed the effect of the drug on the localization of EYFP:AtABCG28 using FM4-64, a marker dye for the plasma membrane and endocytic vesicles, as an internal control. Under control conditions without treatment, EYFP:AtABCG28 colocalized with FM4-64–labeled vesicles only at the tip zone (Fig. 3*A*). After 25 min of treatment with BFA, the EYFP:AtABCG28 signal at the pollen tube tip was much reduced; instead, it appeared as aggregates in the cytosol of the tip region (Fig. 3*B*). The FM4-64 signal changed similarly to EYFP:AtABCG28. After 45 min of treatment with BFA, all EYFP:AtABCG28 signal disappeared from the apical zone (Fig. 3*C*). These results suggest that the apical localization of EYFP:AtABCG28 is BFA-sensitive. In conclusion, AtABCG28 is localized to secretory vesicles in the growing pollen tube and targets to the pollen tube tip.

***atabcg28* Pollen Fail to Elongate Pollen Tubes.** To determine why *atabcg28* pollen failed to produce progeny, we first observed pollen development in *atabcg28*/+ flower buds. There was no apparent defect in the development and maturation of pollen grains in these flowers (Fig. 4*A*), indicating that pollen development is not affected by a loss of *AtABCG28* function. Next, to compare mature *atabcg28*/+ pollen and pollen tubes with those of the wild type, we generated *atabcg28*/+ mutants in the *qrt1*/− background. *qrt1*/− harbors a mutation in the pectin methylesterase gene that blocks the separation of the four pollen grains formed by meiosis and mitosis of one pollen mother cell (54, 55). *atabcg28*/+ *qrt1*/− produced tetrad pollen grains that contained two wild-type pollen grains (AtABCG28) and two *atabcg28* pollen grains that remained stuck together. Tetrads of *atabcg28*/+ *qrt1*/− pollen exhibited four morphologically healthy pollen grains (Fig. 4*B*). Furthermore, the vacuoles of the *atabcg28* mutant pollen grains appeared normal when visualized by neutral red staining (Fig. 4*C*). Thus, we concluded that *atabcg28* mutant pollen developed and matured normally.

We then examined in vitro pollen germination and pollen tube growth (Fig. 4 *D*–*F*). Whereas most of the tetrads produced by *atabcg28*/+ *qrt1*/− plants developed two pollen tubes, most of the *AtABCG28* wild-type tetrads ($^{+/+}$ *qrt1*/−) had three to four pollen tubes. A small portion (8%) of *atabcg28*/+ tetrads produced

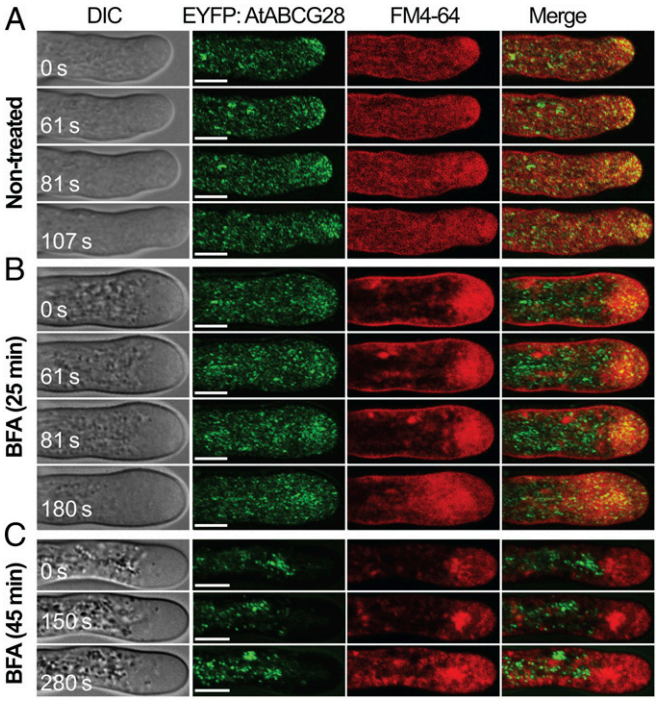

Fig. 3. Targeting of AtABCG28 to the tip is BFA-sensitive. (*A*) Time-lapse images of a control, non-BFA-treated EYFP:AtABCG28 pollen tube stained with the plasma membrane and endocytic marker FM4-64. EYFP:AtABCG28 appears as green dots that move toward the apical zone during tip growth. Note that the EYFP:AtABCG28 signal colocalizes with FM4-64 at the apical zone. (*B* and *C*) Time-lapse images of BFA-treated EYFP:AtABCG28 pollen tubes stained with FM4-64. The pollen were treated with 25 μM BFA for 25 (*B*) or 45 (*C*) min, which stopped their tube growth. t = 0 s marks the beginning of the observation period. An FM4-64–stained, large BFA compartment was apparent. (*B*) EYFP:AtABCG28 signal was much reduced in the apex of the tube compared with the nontreated control shown in *A* and was found in the subapical region, where the BFA compartment was localized. (*C*) After 45 min of treatment with BFA, EYFP:AtABCG28 was absent from the tip and instead appeared as aggregates in the shank, and FM4-64 signal was mostly in the large BFA compartment. Images are representative of three independent experiments. (Scale bars, 5 μm.)

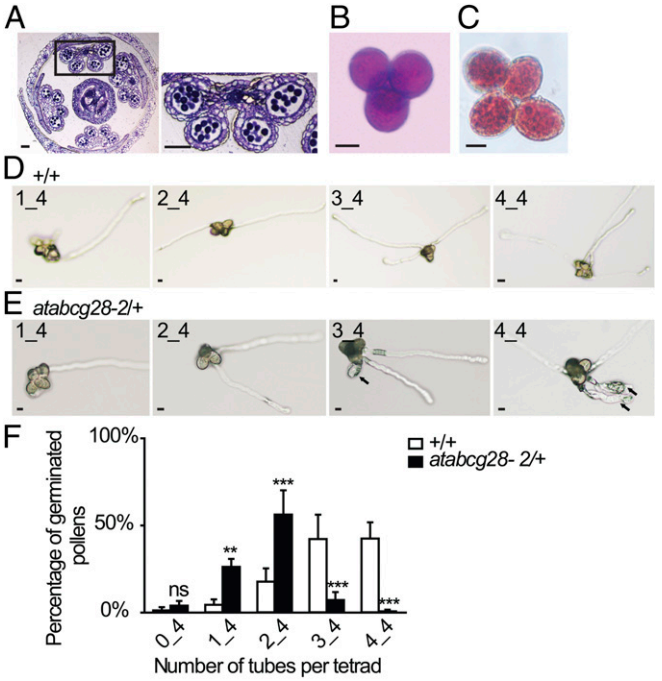

Fig. 4. *atabcg28* knockout mutant pollen develop normally but fail to produce pollen tubes. (*A*) A cross-section of a mature *atabcg28-1*/+ flower just before pollination, stained with toluidine blue. Pollen grains in the pollen sacs of *atabcg28-1*/+ plants appear normal. (Scale bars, 50 μm.) (*B* and *C*) Pollen viability tests of *atabcg28-1*/+ tetrads based on Alexander staining (*B*) and morphology of pollen vacuoles visualized with neutral red (*C*). Note no difference between pollen of different genotypes. (Scale bars, 10 μm.) (*D* and *E*) In vitro-germinated pollen tubes of wild-type (*D*; $^{+/+}$) and *atabcg28*/+ (*E*) tetrads. Arrows indicate *atabcg28* pollen tubes. (Scale bars, 5 μm.) (*F*) Quantitative analysis of in vitro pollen germination of the wild-type ($^{+/+}$) and *atabcg28*/+ tetrads. Error bars are SD. Data were collected from 800 tetrads of the *qrt1* background and 2,000 tetrads of *atabcg28*/+ in four independent experiments. Asterisks indicate statistically significant differences between the wild type and *atabcg28*/+, tested using two-way ANOVA with Bonferroni posttests. ns (not significant), $P > 0.05$; $^{**}P < 0.01$; $^{***}P < 0.001$.

three to four pollen tubes, but all of their third and fourth tubes either burst or were shorter and thicker than those produced by wild-type tetrads (Fig. 4*E*). This result indicated that the *atabcg28* pollen were defective in pollen tube growth. We then studied the reason of the growth defect in *atabcg28* pollen tubes.

***atabcg28* Pollen Tubes Have Altered Hydrogen Peroxide Distribution.** The cysteine-rich N terminus of AtABCG28 (Fig. 1*A*) suggested its potential function in ROS signaling. We examined whether *atabcg28* pollen has any defect in ROS signaling. We first visualized the ROS signal in *atabcg28*/+ tetrad pollen using CM-H_2DCFDA ($DCFH_2$-DA), the most frequently used dye for hydrogen peroxide detection in pollen tube growth (13, 56), and traced the ROS signal using spinning-disk microscopy (57). The representative time-series images of $DCFH_2$-DA presented in Fig. 5*A* show two wild-type pollen exhibiting normal tube elongation (black arrows at $t = 30$ min) and two *atabcg28* pollen, one of which exhibited an emerged tube with no further elongation (red arrowheads) (Fig. 5*A*). We then closely observed two pollen, one wild-type and one *atabcg28* pollen, in a similar focal plane (white arrow and red arrowhead at $t = 0$ min, respectively). In the wild-type pollen, $DCFH_2$-DA fluorescence was concentrated in the tube tip and was weak in the grain (at $t = 10$ and 14 min; Fig. 5 *A* and *B*), as was reported previously (13, 56, 58). By contrast, *atabcg28* had bright fluorescence dispersed throughout the pollen grain (Fig. 5 *A* and *C*–*E*) during the entire observation period (0 to 30 min). The clearly different ROS distribution pattern in *atabcg28* pollen might explain why it failed to elongate. However, the very strong $DCFH_2$-DA signal in pollen might have resulted from its nonspecificity, because it is also oxidized by peroxidases and hemoproteins (59, 60). We therefore visualized H_2O_2 again in the pollen tube by staining with a probe more specific to hydrogen peroxide, pentafluorobenzenesulfonyl fluorescein (PFBSF; refs. 20 and 61). The PFBSF signal was focused to the tip of wild-type pollen tube (Fig. 5*F*) but was dispersed throughout *atabcg28* pollen grain (Fig. 5*G*), much like the signal obtained using $DCFH_2$-DA (Fig. 5*A*).

We then addressed the question of why *atabcg28* and wild-type pollen differed in their patterns of ROS localization. A source of ROS in pollen tubes is the respiratory process in mitochondria, which accumulate at the site of growth to provide energy. Healthy and actively growing pollen tubes are expected to produce ROS, an inevitable by-product of respiration. To test the possibility that the ROS produced by mitochondria might differ between the two pollen genotypes, we used CellRox Deep Red, a dye that detects superoxide and hydroxyl radicals (62). As shown in Fig. 5*I* and *SI Appendix*, Fig. S6, the intensity of the CellRox Deep Red signal did not differ between the wild-type and *atabcg28* pollen, excluding the possibility that mitochondrial activity differed in wild-type and *atabcg28* pollen. Furthermore, close examination of the CellRox Deep Red signal revealed that it was excluded from the apex of the pollen tube (Fig. 5*H*) but was distributed throughout the rest of the pollen tube (Fig. 5 *H* and *I*). This result indicates that the tip-localized ROS signal is not due to superoxide or hydroxyl radicals but to H_2O_2 and, furthermore, that the mitochondrial activity that generates superoxide is not a major contributor to the tip-localized ROS in growing pollen tubes. Finally, the similar levels of CellRox Deep Red signal in wild-type and *atabcg28* pollen (Fig. 5*I* and *SI Appendix*, Fig. S6) indicate that *atabcg28* pollen are as active as the wild-type pollen in terms of mitochondrial activity, excluding the possibility that *atabcg28* pollen are seriously compromised in their basic metabolism, at least during the initial stage of tube growth. Taken together, these results suggested that AtABCG28 is necessary to localize H_2O_2 accumulation to the growing tip, and ROS generated from mitochondria did not contribute much to this specific spatial organization of H_2O_2. We next investigated the localization of polyamine, an important source of H_2O_2, in the pollen tube.

***atabcg28* Pollen Tubes Fail to Accumulate Polyamine in the Tip.** To determine whether the disruption of the tip-localized ROS in *atacbg28* pollen tubes was caused by an altered polyamine localization, we first investigated the distribution of spermine and spermidine (Spm/Spd), the two types of polyamines known to affect pollen tube growth (26, 29), in growing wild-type pollen tubes by immunostaining with an anti-Spm/Spd antibody. Before germination, the Spm/Spd signal was only present in the cell wall (Fig. 6*A*) and not detectable inside (*SI Appendix*, Fig. S7*A*). As soon as pollen started to germinate and elongate the tube, bright signals of intracellular Spm/Spd localized specifically to the tip area in a punctate pattern (Fig. 6 *B* and *C* and *SI Appendix*, Fig. S7 *C* and *D*) and to the cell wall of the tip (Fig. 6*B* and *SI Appendix*, Fig. S7 *B* and *D*).

Next, we examined whether the distribution of Spm/Spd was altered by the *atabcg28* mutation using *atabcg28*/+ tetrads. Before germination, the Spm/Spd signal was observed in the cell walls of *atabcg28*/+ tetrad pollen, and its distribution was similar to that of the wild type in all four pollen grains of the tetrad (Fig. 6 *D* and *E*). However, after germination, the wild-type and *atabcg28* pollen exhibited a distinctly different distribution of Spm/Spd. Two growing pollen tubes of *atabcg28*/+ tetrads (most likely the wild type) exhibited a tip-focused Spm/Spd signal (Fig. 6*G*), similar to that of the four pollen tubes of wild-type tetrads (*qrt1*/−) (Fig. 6*F*). By contrast, two of the *atabcg28*/+ tetrads (most likely *atabcg28*

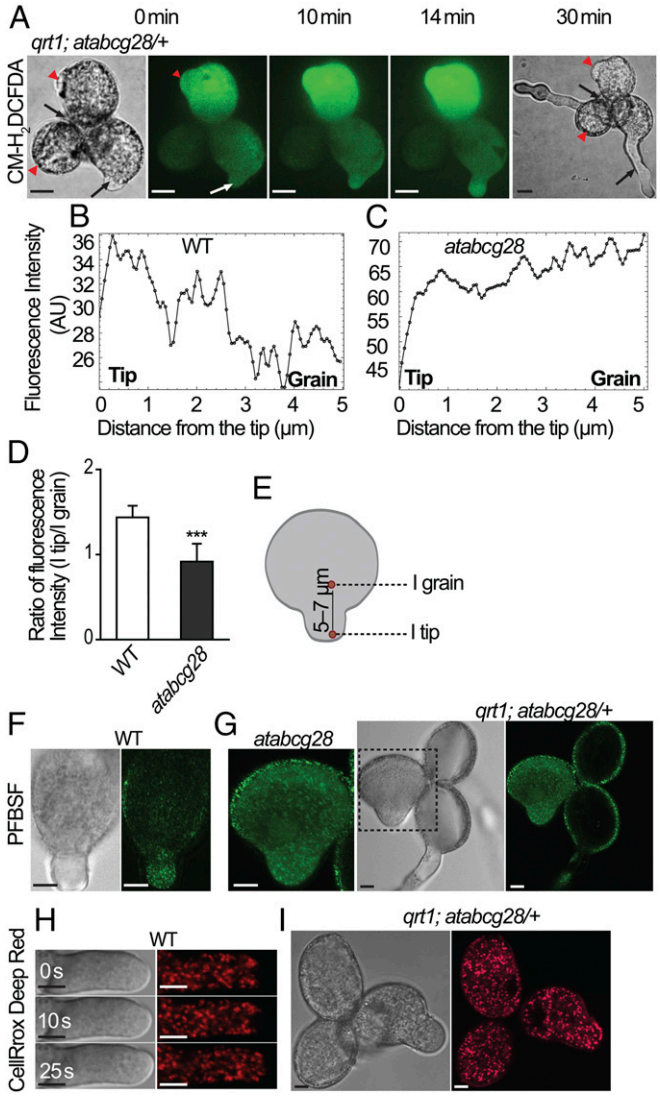

Fig. 5. *atabcg28* pollen tube has dispersed pattern of hydrogen peroxide. (*A*) Time-lapse images of an *atabcg28*/+ tetrad stained with $DCFH_2$-DA. Red arrowheads and black arrows mark *atabcg28* and wild-type pollen, respectively. Red arrowhead and white arrow at $t = 0$ min (the onset of observation) indicate *atabcg28* and wild-type pollen, respectively, in the same focal plane. Note that the green $DCFH_2$-DA signal is focused in the tip of the elongating wild-type pollen tube but is diffuse in *atabcg28* pollen. (Scale bars, 5 μm.) (*B* and *C*) $DCFH_2$-DA fluorescence intensity profiles along the longitudinal axis ($t = 10$ min image) in the wild-type (*B*) and *atabcg28* (*C*) pollen tube, respectively. (*D* and *E*) Ratio of fluorescence intensity in the pollen tube tip (I tip) versus that inside the grain (5 to 7 μm from the tip, I grain) (mean ± SD). Regions in which fluorescence intensity were measured are indicated in *E*. A total of 10~11 wild-type and *atabcg28* pollen were analyzed in three independent experiments. *atabcg28* pollen were chosen from tetrads that had two healthy wild-type pollen tubes. Asterisks denote statistical significance calculated by a by unpaired *t* test (***two-tailed $P < 0.0001$). (*F* and *G*) Hydrogen peroxide distribution in germinated wild-type (*F*) and *atabcg28* (*G*) pollen stained with PFBSF. Note that the green fluorescent signal accumulated in the tip of wild-type pollen but was distributed throughout *atabcg28* pollen. (*H*) Time-lapse images showing the distribution of hydroxyl radical and superoxide in an elongating wild-type pollen tube detected using CellRox Deep Red. Note that the red fluorescent signal of Cell ROx Deep Red is absent from the apex. (*I*) The distribution of hydroxyl radical and superoxide in the early stages of *atabcg28*/+ tetrad germination detected using CellRox Deep Red. Note that there is no difference in the fluorescence intensity and distribution pattern between the three in-focus pollen grains. (Scale bars, 5 μm.)

pollen), regardless of the germination status, exhibited a Spm/Spd signal that was spread throughout the pollen grains (marked with asterisks in Fig. 6*G*). Scanning the fluorescence of the Spm/Spd signal along the long axis of the wild-type pollen tube (Fig. 6 *H*–*J*) confirmed that the Spm/Spd signal was higher at the growing tube tip than inside the grain, whereas it did not differ between the grain and tip in nongrowing cells. These results suggest that *AtABCG28* is essential for establishing a tip-focused distribution of Spm/Spd during pollen tube growth.

Ectopic Expression of *AtABCG28* in Root Hairs Improves Tip Growth at High pH, Most Likely by Mediating Polyamine Secretion. To examine the potential effect of AtABCG28 on polyamine distribution, we ectopically expressed *AtABCG28* in root hairs, which do not express *AtABCG28* (*SI Appendix*, Fig. S1) and thus can be used as a heterologous system for studying tip growth. For this purpose, the root hair-specific Expansin 7A promoter was employed to drive the expression of an EYFP:AtABCG28 coding sequence fusion (*pExp7A*::EYFP:AtABCG28) in *A. thaliana* (*SI Appendix*, Figs. S3*E*, S8, and S9). In the root hair bulge stage, EYFP:AtABCG28 was localized to the plasma membrane (Fig. 7*A*). At this stage, when the tip expansion rate is slow, vesicle trafficking factor ARF-GAP (AGD1) and receptor-like kinase ERULUS similarly localize to the plasma membrane (63, 64). EYFP:AtABCG28 expression did not significantly alter root hair growth under the control growth conditions used, even in the presence of exogenous spermine (*SI Appendix*, Fig. S10). This was not surprising, because the NADPH oxidase RbohC, a major generator of ROS, is active in growing root hairs under normal conditions (11).

We thus analyzed the growth of root hairs in *pExp7A*::EYFP:AtABCG28 plants exposed to higher apoplastic pH values, which inhibit root hair growth (65). Under alkaline conditions, ROS generation by NADPH oxidases is suppressed in root hair cells (65). The inhibition of root hair growth at high pH was confirmed in wild-type plants (*SI Appendix*, Fig. S11). *AtABCG28* expression ameliorated the root hair growth inhibition at high pH; 83 to 96% of three independent lines of AtABCG28-expressing plants developed root hairs, compared with 47% of the wild type at pH 7.5 (*SI Appendix*, Fig. S11). Interestingly, supplementation of the medium with spermine (0.175 mM) restored root hair growth in the wild type to levels of *pExp7A*::EYFP:AtABCG28 plants (Fig. 7 *B* and *C*).

Based on these findings, we hypothesized that the presence of AtABCG28 facilitated polyamine efflux from the cytosol of root hair cells to the apoplast, where PAO catalyzes the oxidation of polyamines to generate hydrogen peroxide and provide the ROS necessary for root hair growth (Fig. 7*D*). If this were the case, the phenotype of AtABCG28 transgenic plants might be reversed when the activity of PAO was inhibited. We tested this possibility using a PAO inactivator, MDL 72527. MDL 72527 is the 2,3-butadienyl derivative of putrescine, which specifically blocks the binding site of spermine and spermidine in PAO (66). Indeed, when the root was treated with the inhibitor at a concentration of 50 μM, root hair growth was reduced to 50% and 75% in two independent AtABCG28 transgenic lines (*SI Appendix*, Fig. S12). This result suggests that the enhanced growth of AtABCG28-expressing root hair cells depends on the activity of PAO.

We then tested whether *AtABCG28* expression also increased ROS levels in root hairs grown at high pH, by measuring ROS levels. Because the root was already expressing EYFP:AtABCG28, which emits green light, we used a red fluorescent dye, CellROX Deep Red, to detect ROS. In the transition zone of the root, after 30 min of staining the CellROX Deep Red signal was mainly detected in the apoplast, but not inside the cell (Fig. 7 *E* and *F*). Thus, in the bulged trichoblasts, in the short-term treatment, the CellROX Deep Red signal mainly detected apoplastic ROS, in contrast to growing pollen tubes, where it only stained intracellular ROS (Fig. 5 *H* and *I* and *SI Appendix*, Fig. S6). The red signal

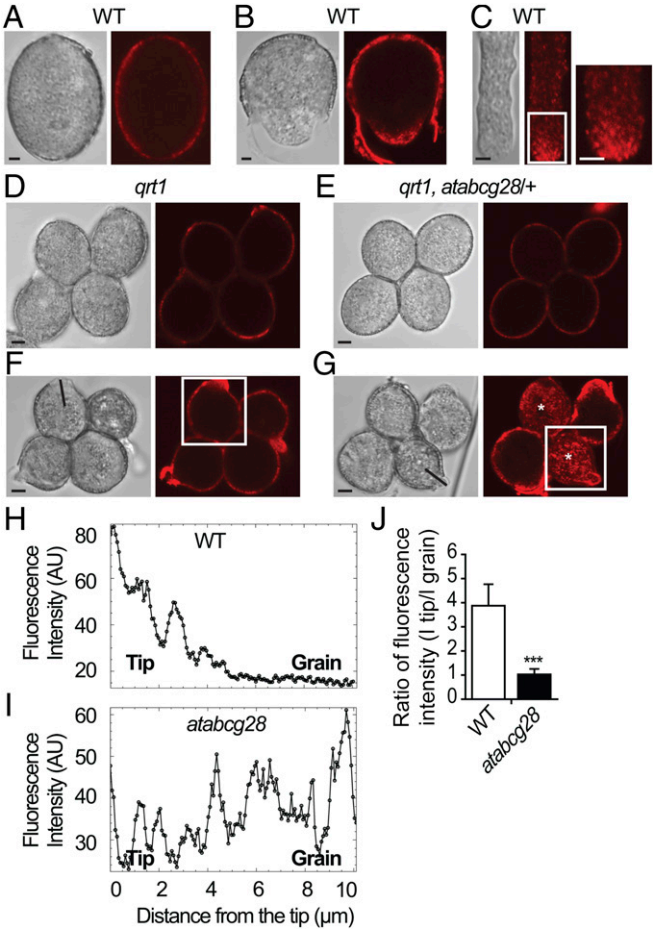

Fig. 6. The tip-focused localization of polyamines is disrupted in *atabcg28* pollen tubes. Polyamines were detected by immunostaining using an antibody that cross-reacts with Spm/Spd. (*A*–*C*) Localization of Spm/Spd in the cell wall of pollen grains (*A* and *B*) and in the tips of elongating pollen tubes (*B* and *C*). Elongating pollen tubes exhibit a Spm/Spd signal in an inverted cone shape. Enlargement of boxed region (*C*, *Inset*) showing the dotted distribution of polyamine in the apical clear zone. (*D*, *F*, and *H*) Representative localization of Spm/Spd in the wild-type tetrads (*qrt1*). Pollen soon after germination without and with an emerged tube (*D*); a tetrad with an elongated pollen tube (*F*); fluorescence intensity profile measured along the pollen tube axis (*H*), indicated in *F*. Note that Spm/Spd localization is focused on the growth sites in pollen grains and tubes. (*E*, *G*, and *I*) Representative localizations of Spm/Spd observed in *atabcg28*/+ tetrads. A nongerminated *atabcg28*/+ tetrad exhibiting cell wall localization of Spm/Spd (*E*), which is indistinguishable between the wild-type and *atabcg28* pollen grains; an *atabcg28*/+ tetrad soon after germination (*G*), which had two germinated wild-type pollen and two germinated *atabcg28* pollen (asterisks). Fluorescence intensity profile (*I*) measured along the *atabcg28* pollen tube axis, indicated in *G*. Note that Spm/Spd is dispersed throughout *atabcg28* pollen grains and tubes as germination progresses. (*J*) Ratio of fluorescence intensity value in the tip (I tip) compared with that inside the grain region (5 to 7 μm from the tip, I grain) of the pollen tube (mean ± SD). Positions at which fluorescence intensity were measured are indicated in Fig. 5*E*. A total of 22 wild-type and *atabcg28* tetrads were analyzed in three independent experiments. *atacbg28* pollen were chosen from tetrads that had two healthy wild-type pollen tubes. Asterisks denote statistical significance calculated by an unpaired *t* test (***two-tailed $P < 0.0001$). (Scale bars, 2.5 μm.)

observed was not due to autofluorescence, as the cell wall of the nonstained root did not fluoresce under the conditions of this experiment (*SI Appendix*, Fig. S13). As shown in Fig. 7 *E*–*G*, the ROS level was higher in *pExp7A*::*EYFP:AtABCG28* root hairs than in wild-type root hairs. These results are consistent with our hypothesis that AtABCG28 expressed in root hair cells increases ROS levels by facilitating polyamine transfer to the apoplast, and thereby rescues root hair growth at pH 7.5.

Discussion

In this study, we identified an ABC protein, AtABCG28, which is essential for pollen fertility. It establishes the tip-localized accumulation of H_2O_2 during pollen tube growth. In addition,

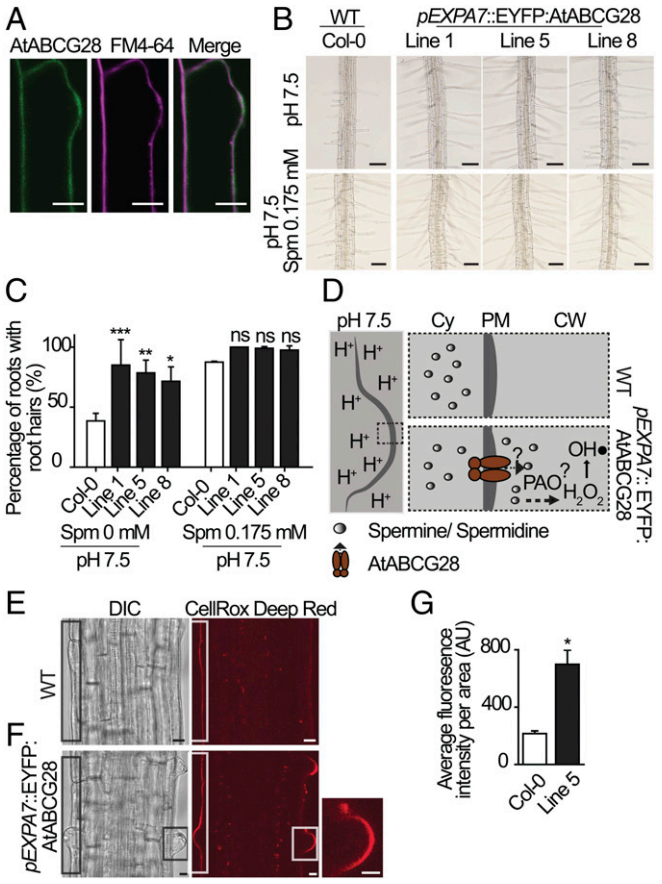

Fig. 7. Ectopic expression of *AtABCG28* improves root hair elongation at high pH. (*A*) Plasma membrane localization of AtABCG28 in a bulging root hair cell. The EYFP:AtABCG28 signal was higher than in other regions of the root hair when the hair bulge emerged. (Scale bars, 10 μm.) (*B*) Representative root hair images of the wild-type (Col-0) and three independent *pEXP7*::EYFP:AtABCG28 transgenic lines grown in 1/8 MS-agar medium at pH 7.5 with or without spermine (0.175 mM). (Scale bars, 100 μm.) (*C*) Percentage values of roots with elongated root hairs at pH 7.5 in the absence or presence of 0.175 mM spermine. Data (mean ± SD) from two independent experiments ($n = 50$ roots per genotype) are presented. Asterisks denote statistical significance between wild-type and transgenic lines, calculated by two-way ANOVA and Bonferroni posttests [*$P < 0.05$; **$P < 0.01$; ***$P < 0.001$; ns (not significant), $P > 0.05$]. (*D*) A model for the expected function of AtABCG28 in root hair growth at high pH conditions. The dashed inset is a proposed model explaining the difference in development of trichoblast cells between wild-type and transgenic plants expressing *AtABCG28*. At high pH, spermine and spermidine synthesized in the cytosol are secreted to the apoplast by AtABCG28 and oxidized into hydrogen peroxide (H_2O_2) by the activity of PAO. Hydrogen peroxide is further catalyzed into its hydroxyl radical, which loosens the cell wall and thus stimulates root hair elongation. (*E* and *F*) Representative images of ROS signal visualized with CellRox Deep Red in the differentiation zone of the Col-0 root (*E*) and *pEXP7*::EYFP:AtABCG28 line 5 (*F*). (*F*, *Inset*) Enlargement of hair bulge. (Scale bars, 10 μm.) (*G*) Relative ROS levels (mean ± SD) quantified in the wild-type (Col-0) and *pEXP7*:: EYFP:AtABCG28 (line 5) roots. Fourteen roots per genotype from two independent experiments were analyzed. Asterisk denotes statistical significance between wild-type and transgenic line, calculated by an unpaired *t* test (*two-tailed $P < 0.05$).

we visualized the localization of endogenous Spm/Spd in the secretory vesicles and cell wall of the apex of growing pollen tube. This localization pattern coincided with that of H_2O_2 and AtABCG28 and depended on AtABCG28 function. We speculate that AtABCG28 either transports polyamine into secretory vesicles or is involved in trafficking of the secretory vesicles to the growing tip. Such functions of AtABCG28 could concentrate H_2O_2 to a high level at the pollen tube tip, where the vesicles accumulate. In addition, such compartmentation of polyamines would protect the cytosol from polyamine toxicity and guide polyamines to the pollen tube tip. When vesicles fuse to the tip, polyamines are likely to be released into the apoplast, where they are deposited into the cell wall as stable components.

AtABCG28 Contributes to the Tip-Focused Accumulation of Polyamines That Is Associated with Pollen Tube Growth. Although the intracellular localization of polyamines in plants has not been studied in detail, polyamines have been shown to play crucial roles in pollen, from gametophyte development to fertilization (67). In particular, polyamines regulate the generation of ROS and Ca^{2+} gradients and maintain cell wall integrity during pollen tube growth (26, 28). However, the mechanism by which polyamines synthesized in the cytosol are transported to the pollen tube tip and cell wall was hitherto unknown.

Four lines of experimental evidence presented here suggest that polyamines are secreted from the pollen tube apex and that AtABCG28 is essential for the secretion process. First, immunostaining with anti-Spm/Spd revealed that Spm/Spd are localized to secretory vesicles, which are distributed in an inverted cone pattern in growing pollen tube tips (Fig. 6), and this pattern resembles the localization of AtABCG28 in growing pollen tubes (Figs. 2*C* and 3 and *SI Appendix*, Fig. S5). Second, loss of AtABCG28 function disrupted the tip-focused distribution of Spm/Spd in the pollen tube (Fig. 6 *G*, *I*, and *J*), indicating that AtABCG28 function is essential for the translocation of Spm/Spd to the growing pollen tube tip. Third, the growth-promoting effect of ectopic *AtABCG28* expression in root hairs at alkaline pH (Fig. 7 *B* and *C* and *SI Appendix*, Fig. S11) was abolished by an inhibitor of PAO (*SI Appendix*, Fig. S12), indicating that the effect of *AtABCG28* expression depends on polyamines. Fourth, at high pH, an external supply of spermine promoted the growth of the wild-type root hairs to rates measured in *AtABCG28*-expressing root hairs (Fig. 7 *B* and *C*), suggesting that the growth promotion mediated by ectopically expressed AtABCG28 might also be mediated by polyamine at the apoplast.

Furthermore, this apical accumulation of Spm/Spd seemed to be important for pollen tube elongation since it was always associated with elongating pollen tubes, and never with the nonelongating ones (Fig. 6). The role of polyamine distribution in directional movement was shown recently in migrating animal cells. When weak electric fields guided cell migration, the intracellular distribution of Spm/Spd became asymmetrical, with the highest concentration at the growing side of the cell (the leading edge) (68).

AtABCG28-Mediated Asymmetrical Polyamine Distribution Establishes the Tip-Focused ROS. Multiple sources of ROS were suggested to exist in growing pollen tubes, including NADPH oxidases and polyamines (14–16, 26). Our results indicate that the tip-focused Spm/Spd distribution mediated by AtABCG28 is essential for tip-focused ROS generation. In *atabcg28* pollen, ROS, visualized using $DCFH_2$-DA and PFBSF, was distributed throughout the pollen grains (Fig. 5), and Spm/Spd distribution was similarly altered (Fig. 6). The tight coupling of ROS and Spm/Spd suggests that Spm/Spd are used to produce ROS in this cell. Similar coupling of ROS and polyamine was also found in root hair cells expressing AtABCG28; ROS levels and the ability to grow at high pH were increased in the root hairs of plants ectopically expressing *AtABCG28* (Fig. 7), and this was abolished when ROS generation from polyamines was blocked by PAO inhibitor (*SI Appendix*, Fig. S12).

Our results suggest that the failure to establish the tip-focused ROS in *atabcg28* pollen is the reason why it could not elongate after initial bulging. Although the overall high ROS observed in newly germinated *atabcg28* pollen stained with $DCFH_2$-DA raised a possibility that high ROS might have inhibited pollen tube elongation, staining with more specific dyes for ROS, PFBSF and CellRox DeepRed, revealed that ROS levels and mitochondrial activity in *atabcg28* pollen tubes did not differ much from those in the wild type during the early stage of pollen tube growth (Fig. 5 *G* and *I* and *SI Appendix*, Fig. S6). Thus, it is likely that the altered distribution of hydrogen peroxide was the major cause for *atabcg28* defects at the beginning of pollen tube growth.

We postulate that the complete male sterility of an *atabcg28* loss-of-function mutant (Tables 1 and 2) is due to the critical importance of ROS derived from Spm/Spd enveloped in secretory vesicles for pollen tube elongation. Pollen tubes derived from *atabcg28* rarely elongated (Fig. 4), due to alterations in ROS (Fig. 5) and Spm/Spd distribution patterns (Fig. 6). By contrast, the knockout of pollen-specific NADPH oxidase genes caused only partial male sterility, and did not abolish elongation of the pollen tube (15, 16). It is possible that NADPH oxidases contribute to ROS generation at a later stage of pollen tube growth than the polyamine system we describe here.

Models for the Function of AtABCG28 in Pollen Tube Growth. In the newly germinated wild-type pollen Spm/Spd and H_2O_2 were localized specifically at the growing tip, whereas in *atabcg28* pollen they were dispersed throughout the pollen cytosol (Figs. 5 and 6).

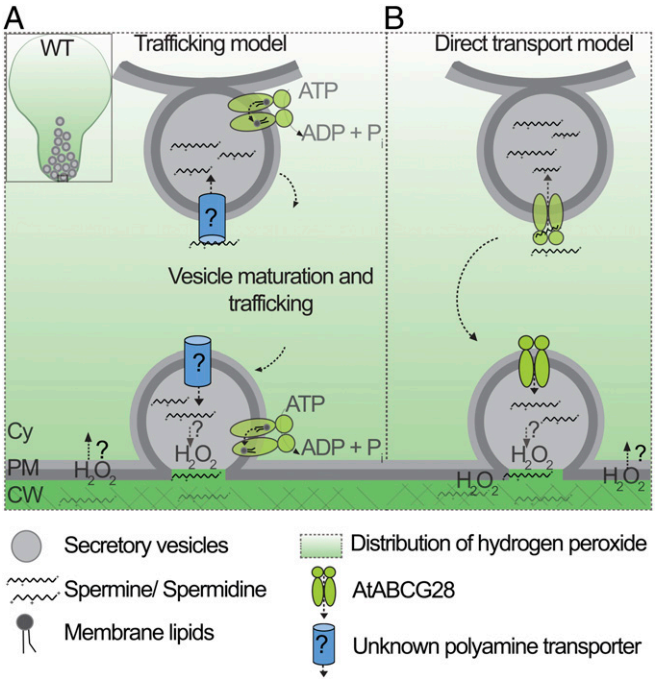

Fig. 8. Proposed working models of AtABCG28 function during pollen tube growth. (*A*) Trafficking model: AtABCG28 might be involved in trafficking of the secretory vesicles to the tip of the growing pollen tube. An unknown polyamine transporter mediates Spm/Spd loading into the secretory vesicles, and AtABCG28 facilitates trafficking of Spm/Spd containing vesicles to the apical zone, possibly by transporting a so far unidentified substrate. (*B*) Direct transport model: AtABCG28 might directly transport Spm/Spd from the cytosol into secretory vesicles which move to the tip of the pollen tube. AtABCG28-mediated loading of Spm/Spd molecules into the secretory vesicles protects the cytosol from the cytotoxicity of polyamines. Sequestered Spm/Spd are oxidized, producing H_2O_2, or released into the apoplast, where H_2O_2 is generated during pollen tube growth. Cy, cytosol; SV, secretory vesicle; PM, plasma membrane.

Based on these observations, we speculate two possible functions of AtABCG28 (Fig. 8): either AtABCG28 acts as a component necessary for trafficking of secretory vesicles containing Spm/Spd or it acts as a transporter of polyamine. According to the first model (Fig. 8*A*), a so-far-unknown transporter loads Spm/Spd into the secretory vesicles, whereas AtABCG28 facilitates trafficking and delivery of the polyamine containing vesicles to the apex of the pollen tube. In support of this model, a number of mammalian half-size ABC transporters function as membrane lipid floppase at the stages of vesicle scission or fusion (69) and AtABCG28 could have a similar function. The model predicts that PAO localizes in secretory vesicles rather than in the cytosol. There is not yet any evidence for the localization of PAO in secretory vesicles of the pollen tube.

According to the second model (Fig. 8*B*), AtABCG28 directly transports Spm/Spd into the secretory vesicles that eventually release their contents to the apoplast upon fusion of the vesicles to the plasma membrane. In strong support of this model, AtABCG28 contains multiple thiol groups, which is expected for a protein directly involved in handling ROS-related compounds. According to this model, *atabcg28* mutant pollen would fail to sequester Spm/Spd into secretory vesicles such that free Spm/Spd electrostatically can interact with cellular components such as nucleic acids, proteins, and membrane lipids in a nonselective manner (31, 32). Formation of aggregates containing Spm/Spd throughout the cytosol would explain the punctuated pattern visualized under microscopy in *atabcg28* mutant pollen tubes (Figs. 5*G* and 6*G*). Although we favor this second model, biochemical evidence that AtABCG28 directly transports Spm/Spd is lacking, and further studies are required to resolve which of the two models is correct.

Physiological Role of Many Cysteines in the N-Terminal Noncytoplasmic Domain of AtABCG28. An intriguing question is why there are so many cysteine residues in the N-terminal noncytoplasmic domain of the AtABCG28 transporter. The existence of numerous cysteines, especially the four heme regulatory cysteine–proline motifs, is common in proteins that control cellular redox status such as cytochromes (70). It has been suggested that cysteines in such proteins could act as redox sensors (71), and we therefore envision that the cysteine residues of AtABCG28 might carry out a similar function. The cysteine residues may undergo reversible thiol oxidation in response to changes in the oxidation status in the lumen of secretory vesicles or the apoplast, likely linking the activity of the AtABCG28 transporter to the control of cellular redox status required for pollen tube growth.

Possible Functions of Polyamines in Root Hair Growth. Root hair growth under standard growth conditions (pH 5.7) depends on substantial levels of ROS generated by NADPH oxidases; a knockout of the NADPH oxidase RbohC severely inhibits root hair growth (11). However, root hair growth is restored in *rbohC* mutants at slightly alkaline conditions, indicating the existence of alternative mechanisms that support root hair growth (65).

Polyamines are important sources of ROS generated during root development (72) and are suggested to regulate plant growth under stress (73). Polyamines are secreted to the apoplast under stress conditions (74). However, it was previously unknown whether polyamines are important for root hair development. Our results suggest that polyamines are required for root hair growth under slightly alkaline conditions (pH 7.5; Fig. 7 and *SI Appendix*, Figs. S11 and S12). At this pH, wild-type *Arabidopsis* plants exhibited reduced root hair growth (Fig. 7 and *SI Appendix*, Fig. S11). Externally supplied polyamines enhanced root hair growth at pH 7.5 (Fig. 7). Overexpression of *AtABCG28* increased ROS levels in root hair cells at pH 7.5 (Fig. 7) and increased root hair growth, which was again suppressed by PAO inhibitor (*SI Appendix*, Fig. S12). However, neither external polyamines nor *AtABCG28* expression promoted root hair growth at pH 5.7 (*SI Appendix*, Fig. S10). These data collectively indicate that ROS generated from polyamines contribute to root hair growth at slightly alkaline pH.

In summary, we identified an ABC protein that mediates the asymmetrical distribution of polyamines inside a single cell. This activity is critical for reproductive success of the male gamete in *Arabidopsis*. Thus, this work reveals another important player in plant reproduction.

Materials and Methods

In Vitro Pollen Germination, ROS Detection, and BFA Treatment. In vitro pollen germination was examined in medium containing 10% (wt/vol) sucrose, 0.01% (wt/vol) boric acid, 5 mM potassium chloride, 5 mM calcium chloride, 1 mM magnesium chloride, and 1.5% (wt/vol) agarose for the *quartet* background (75). The germination rate of the wild type and mutant was calculated at 6 h after the start of germination. To observe ROS levels, tetrad pollen grains were germinated on a slide containing germination medium for 1~3 h and stained in 200 μL of germination medium containing 10 μM CM-H_2DCFDA (C6827; Invitrogen) for 5 min, 10 μM pentafluorobenzenesulfonyl fluorescein (728912-45-6; Cayman) for 10 min, or 5 μM CellROX Deep Red Reagent (C10422; Invitrogen) for 30 min.

For BFA treatment, germinating pollen were loaded first with 12 μM FM4-64 (T13320; Invitrogen) at room temperature. After 6 to 10 min, the dye was removed, and the samples were treated with 25 μM BFA (Sigma) for 10 to 90 min.

Immunostaining of Polyamines in Pollen Tubes. Immunostaining of intracellular polyamines in the pollen tube was performed as described in refs. 76 and 77 with some modifications. To facilitate penetration of the primary antibody into the cell, pollen tubes were digested with 0.1% pectinase (vol/vol) and 1% cellulase (wt/vol) for 6 h. The pollen sample was then incubated in TBS with 0.002% (wt/vol) saponin at 4 °C overnight, blocked in TBS with 0.002% (wt/vol) saponin and 5% (wt/vol) BSA for 1 h at room temperature (RT), and then further incubated in TBS with 0.002% (wt/vol) saponin, 1% (wt/vol) BSA, and anti-spermine polyclonal antibody (1:50 dilution, ab26975; Abcam) overnight. Vacuum was applied to the samples 15 to 30 min before washing out the primary antibody. Finally, samples were incubated with goat anti-rabbit IgG (H+L) cross-adsorbed secondary antibody and Alexa Fluor 568 (1:500 dilution, A11011; Invitrogen) for 1 h at RT.

For other methods see *SI Appendix, Materials and Methods*.

ACKNOWLEDGMENTS. We thank professor Yumi Kim for the use of the spinning disk confocal microscopy. This research was supported by Basic Science Research Program NRF-2018R1A2A1A05018173 (to Y.L.), through the National Research Foundation of Korea funded by the Ministry of Science and ICT (Information and Communication Technology).

1. B. Halliwell, Reactive species and antioxidants. Redox biology is a fundamental theme of aerobic life. *Plant Physiol.* **141**, 312–322 (2006).
2. S. Neill, R. Desikan, J. Hancock, Hydrogen peroxide signalling. *Curr. Opin. Plant Biol.* **5**, 388–395 (2002).
3. S. Mangano, S. P. D. Juárez, J. M. Estevez, ROS regulation of polar growth in plant cells. *Plant Physiol.* **171**, 1593–1605 (2016).
4. C. P. Semighini, S. D. Harris, Regulation of apical dominance in Aspergillus nidulans hyphae by reactive oxygen species. *Genetics* **179**, 1919–1932 (2008).
5. S. M. Coelho, C. Brownlee, J. H. Bothwell, A tip-high, Ca(2+) -interdependent, reactive oxygen species gradient is associated with polarized growth in fucus serratus zygotes. *Planta* **227**, 1037–1046 (2008).
6. T. R. Hurd, M. DeGennaro, R. Lehmann, Redox regulation of cell migration and adhesion. *Trends Cell Biol.* **22**, 107–115 (2012).
7. Z.-M. Pei *et al*., Calcium channels activated by hydrogen peroxide mediate abscisic acid signalling in guard cells. *Nature* **406**, 731–734 (2000).
8. V. Demidchik, ROS-activated ion channels in plants: Biophysical characteristics, physiological functions and molecular nature. *Int. J. Mol. Sci.* **19**, E1263 (2018).
9. G. P. Bienert, J. K. Schjoerring, T. P. Jahn, Membrane transport of hydrogen peroxide. *Biochim. Biophys. Acta* **1758**, 994–1003 (2006).
10. M. Ushio-Fukai, Compartmentalization of redox signaling through NADPH oxidase-derived ROS. *Antioxid. Redox Signal.* **11**, 1289–1299 (2009).
11. J. Foreman *et al*., Reactive oxygen species produced by NADPH oxidase regulate plant cell growth. *Nature* **422**, 442–446 (2003).
12. R. J. Carol *et al*., A RhoGDP dissociation inhibitor spatially regulates growth in root hair cells. *Nature* **438**, 1013–1016 (2005).

13. M. Potocký, M. A. Jones, R. Bezvoda, N. Smirnoff, V. Zárský, Reactive oxygen species produced by NADPH oxidase are involved in pollen tube growth. *New Phytol.* **174**, 742–751 (2007).
14. J. Wu *et al.*, Spermidine oxidase-derived H_2O_2 regulates pollen plasma membrane hyperpolarization-activated Ca(2+) -permeable channels and pollen tube growth. *Plant J.* **63**, 1042–1053 (2010).
15. Kaya H, *et al.* Ca2+-activated reactive oxygen species production by Arabidopsis RbohH and RbohJ is essential for proper pollen tube tip growth. *Plant Cell* **26**, 1069–1080 (2014).
16. R. Lassig, T. Gutermuth, T. D. Bey, K. R. Konrad, T. Romeis, Pollen tube NAD(P)H oxidases act as a speed control to dampen growth rate oscillations during polarized cell growth. *Plant J.* **78**, 94–106 (2014).
17. H. Kaya *et al.*, Apoplastic ROS production upon pollination by RbohH and RbohJ in Arabidopsis. *Plant Signal. Behav.* **10**, e989050 (2015).
18. G. P. Bienert, F. Chaumont, Aquaporin-facilitated transmembrane diffusion of hydrogen peroxide. *Biochim. Biophys. Acta* **1840**, 1596–1604 (2014).
19. A. Speranza, R. Crinelli, V. Scoccianti, A. Geitmann, Reactive oxygen species are involved in pollen tube initiation in kiwifruit. *Plant Biol. (Stuttg)* **14**, 64–76 (2012).
20. N. Maksimov, A. Evmenyeva, M. Breygina, I. Yermakov, The role of reactive oxygen species in pollen germination in Picea pungens (blue spruce). *Plant Reprod.* **31**, 357–365 (2018).
21. A. J. Michael, Polyamines in eukaryotes, bacteria and archaea. *J. Biol. Chem.* **291**, 14896–14903 (2016).
22. T. A. Smith, Polyamines. *Annu. Rev. Plant Physiol.* **36**, 117–143 (1985).
23. N. Bagni, P. Adamo, D. Serafini-Fracassini, V. R. Villanueva, RNA, proteins and polyamines during tube growth in germinating apple pollen. *Plant Physiol.* **68**, 727–730 (1981).
24. G. Falasca, M. Franceschetti, N. Bagni, M. M. Altamura, R. Biasi, Polyamine biosynthesis and control of the development of functional pollen in kiwifruit. *Plant Physiol. Biochem.* **48**, 565–573 (2010).
25. P. Fincato *et al.*, The members of Arabidopsis thaliana PAO gene family exhibit distinct tissue- and organ-specific expression pattern during seedling growth and flower development. *Amino Acids* **42**, 831–841 (2012).
26. I. Aloisi, G. Cai, V. Tumiatti, A. Minarini, S. Del Duca, Natural polyamines and synthetic analogs modify the growth and the morphology of Pyrus communis pollen tubes affecting ROS levels and causing cell death. *Plant Sci.* **239**, 92–105 (2015).
27. F. Antognoni, N. Bagni, Bis(guanylhydrazones) negatively affect in vitro germination of kiwifruit pollen and alter the endogenous polyamine pool. *Plant Biol (Stuttg)* **10**, 334–341 (2008).
28. I. Aloisi *et al.*, Spermine regulates pollen tube growth by modulating Ca2+-dependent actin organization and cell wall structure. *Front. Plant Sci.* **8**, 1701 (2017).
29. M. J. Rodriguez-Enriquez, S. Mehdi, H. G. Dickinson, R. T. Grant-Downton, A novel method for efficient in vitro germination and tube growth of Arabidopsis thaliana pollen. *New Phytol.* **197**, 668–679 (2013).
30. Y. Takeda *et al.*, Determination of protonation sites in thermospermine and in some other polyamines by 15N and 13C nuclear magnetic resonance spectroscopy. *Eur. J. Biochem.* **130**, 383–389 (1983).
31. R. D. Slocum, H. E. Flores, *Biochemistry and Physiology of Polyamines in Plants* (CRC Press, 1991).
32. E. Agostinelli *et al.*, Polyamines: Fundamental characters in chemistry and biology. *Amino Acids* **38**, 393–403 (2010).
33. M. Fujita, K. Shinozaki, Identification of polyamine transporters in plants: Paraquat transport provides crucial clues. *Plant Cell Physiol.* **55**, 855–861 (2014).
34. A. A. Abdulhussein, H. M. Wallace, Polyamines and membrane transporters. *Amino Acids* **46**, 655–660 (2014).
35. M. Hiasa *et al.*, Identification of a mammalian vesicular polyamine transporter. *Sci. Rep.* **4**, 6836 (2014).
36. T. Takeuchi *et al.*, Vesicular polyamine transporter mediates vesicular storage and release of polyamine from mast cells. *J. Biol. Chem.* **292**, 3909–3918 (2017).
37. K. Igarashi, K. Kashiwagi, Polyamine transport in bacteria and yeast. *Biochem. J.* **344**, 633–642 (1999).
38. L. Miller-Fleming, V. Olin-Sandoval, K. Campbell, M. Ralser, Remaining mysteries of molecular biology: The role of polyamines in the cell. *J. Mol. Biol.* **427**, 3389–3406 (2015).
39. M. Fujita *et al.*, Natural variation in a polyamine transporter determines paraquat tolerance in Arabidopsis. *Proc. Natl. Acad. Sci. U.S.A.* **109**, 6343–6347 (2012).
40. J. Li *et al.*, Paraquat resistant1, a golgi-localized putative transporter protein, is involved in intracellular transport of paraquat. *Plant Physiol.* **162**, 470–483 (2013).
41. M. Fujita, K. Shinozaki, "Polyamine transport systems in plants" in *Polyamines*, T. Kusano, H. Suzuki, Eds. (Springer, 2015), pp. 179–185.
42. J. Xi, P. Xu, C. B. Xiang, Loss of AtPDR11, a plasma membrane-localized ABC transporter, confers paraquat tolerance in Arabidopsis thaliana. *Plant J.* **69**, 782–791 (2012).
43. F. L. Theodoulou, I. D. Kerr, ABC transporter research: Going strong 40 years on. *Biochem. Soc. Trans.* **43**, 1033–1040 (2015).
44. M. Klein *et al.*, The ATP-binding cassette (ABC) transporter Bpt1p mediates vacuolar sequestration of glutathione conjugates in yeast. *FEBS Lett.* **520**, 63–67 (2002).
45. E. Desuzinges-Mandon *et al.*, ABCG2 transports and transfers heme to albumin through its large extracellular loop. *J. Biol. Chem.* **285**, 33123–33133 (2010).
46. G. Zhao, J. Shi, W. Liang, D. Zhang, ATP binding cassette G transporters and plant male reproduction. *Plant Signal. Behav.* **11**, e1136764 (2016).
47. L. B. Poole, K. J. Nelson, Discovering mechanisms of signaling-mediated cysteine oxidation. *Curr. Opin. Chem. Biol.* **12**, 18–24 (2008).
48. R. Schwacke *et al.*, ARAMEMNON, a novel database for Arabidopsis integral membrane proteins. *Plant Physiol.* **131**, 16–26 (2003).
49. K. W. Bock *et al.*, Integrating membrane transport with male gametophyte development and function through transcriptomics. *Plant Physiol.* **140**, 1151–1168 (2006).
50. J. Derksen *et al.*, Quantitative analysis of the distribution of organelles in tobacco pollen tubes: Implications for exocytosis and endocytosis. *Protoplasma* **188**, 267–276 (1995).
51. R. M. Parton, S. Fischer-Parton, A. J. Trewavas, M. K. Watahiki, Pollen tubes exhibit regular periodic membrane trafficking events in the absence of apical extension. *J. Cell Sci.* **116**, 2707–2719 (2003).
52. Q. Wang *et al.*, Effects of brefeldin A on pollen germination and tube growth. antagonistic effects on endocytosis and secretion. *Plant Physiol.* **139**, 1692–1703 (2005).
53. A. Nebenführ, C. Ritzenthaler, D. G. Robinson, Brefeldin A: Deciphering an enigmatic inhibitor of secretion. *Plant Physiol.* **130**, 1102–1108 (2002).
54. D. Preuss, S. Y. Rhee, R. W. Davis, Tetrad analysis possible in Arabidopsis with mutation of the QUARTET (QRT) genes. *Science* **264**, 1458–1460 (1994).
55. S. A. Johnson-Brousseau, S. McCormick, A compendium of methods useful for characterizing Arabidopsis pollen mutants and gametophytically-expressed genes. *Plant J.* **39**, 761–775 (2004).
56. C.-L. Wang *et al.*, S-RNase disrupts tip-localized reactive oxygen species and induces nuclear DNA degradation in incompatible pollen tubes of Pyrus pyrifolia. *J. Cell Sci.* **123**, 4301–4309 (2010).
57. S. L. Hempel, G. R. Buettner, Y. Q. O'Malley, D. A. Wessels, D. M. Flaherty, Dihydrofluorescein diacetate is superior for detecting intracellular oxidants: Comparison with 2′,7′-dichlorodihydrofluorescein diacetate, 5(and 6)-carboxy-2′,7′-dichlorodihydrofluorescein diacetate, and dihydrorhodamine 123. *Free Radic. Biol. Med.* **27**, 146–159 (1999).
58. J. K. Muhlemann, T. L. B. Younts, G. K. Muday, Flavonols control pollen tube growth and integrity by regulating ROS homeostasis during high-temperature stress. *Proc. Natl. Acad. Sci. U.S.A.* **115**, E11188–E11197 (2018).
59. C. Rota, C. F. Chignell, R. P. Mason, Evidence for free radical formation during the oxidation of 2′-7′-dichlorofluorescin to the fluorescent dye 2′-7′-dichlorofluorescein by horseradish peroxidase: Possible implications for oxidative stress measurements. *Free Radic. Biol. Med.* **27**, 873–881 (1999).
60. T. Ohashi *et al.*, Rapid oxidation of dichlorodihydrofluorescin with heme and hemoproteins: Formation of the fluorescein is independent of the generation of reactive oxygen species. *FEBS Lett.* **511**, 21–27 (2002).
61. H. Maeda *et al.*, Fluorescent probes for hydrogen peroxide based on a non-oxidative mechanism. *Angew. Chem. Int. Ed. Engl.* **43**, 2389–2391 (2004).
62. M. Alves *et al.*, An efficient technique to detect sperm reactive oxygen species: The CellRox deep red fluorescent probe. *Biochem. Physiol.* **4**, 157 (2015).
63. C.-M. Yoo *et al.*, Deletion analysis of AGD1 reveals domains crucial for plasma membrane recruitment and function in root hair polarity. *J. Cell Sci.* **131**, jcs203828 (2018).
64. T. Kwon, J. A. Sparks, F. Liao, E. B. Blancaflor, ERULUS is a plasma membrane-localized receptor-like kinase that specifies root hair growth by maintaining tip-focused cytoplasmic calcium oscillations. *Plant Cell* **30**, 1173–1177 (2018).
65. G. B. Monshausen, T. N. Bibikova, M. A. Messerli, C. Shi, S. Gilroy, Oscillations in extracellular pH and reactive oxygen species modulate tip growth of Arabidopsis root hairs. *Proc. Natl. Acad. Sci. U.S.A.* **104**, 20996–21001 (2007).
66. N. Seiler, B. Duranton, F. Raul, The polyamine oxidase inactivator MDL 72527. *Prog. Drug Res.* **59**, 1–40 (2002).
67. I. Aloisi, G. Cai, D. Serafini-Fracassini, S. Del Duca, Polyamines in pollen: From microsporogenesis to fertilization. *Front. Plant Sci.* **7**, 155 (2016).
68. K. I. Nakajima *et al.*, KCNJ15/Kir4.2 couples with polyamines to sense weak extracellular electric fields in galvanotaxis. *Nat. Commun.* **6**, 8532 (2015).
69. E. J. Tarling, T. Q. de Aguiar Vallim, P. A. Edwards, Role of ABC transporters in lipid transport and human disease. *Trends Endocrinol. Metab.* **24**, 342–350 (2013).
70. H. M. Girvan, A. W. Munro, Heme sensor proteins. *J. Biol. Chem.* **288**, 13194–13203 (2013).
71. J. A. Traverso, A. Pulido, M. I. Rodríguez-García, J. D. D. Alché, Thiol-based redox regulation in sexual plant reproduction: New insights and perspectives. *Front. Plant Sci.* **4**, 465 (2013).
72. A. Tisi *et al.*, Perturbation of polyamine catabolism can strongly affect root development and xylem differentiation. *Plant Physiol.* **157**, 200–215 (2011).
73. T. Capell, L. Bassie, P. Christou, Modulation of the polyamine biosynthetic pathway in transgenic rice confers tolerance to drought stress. *Proc. Natl. Acad. Sci. U.S.A.* **101**, 9909–9914 (2004).
74. P. N. Moschou *et al.*, Spermidine exodus and oxidation in the apoplast induced by abiotic stress is responsible for H2O2 signatures that direct tolerance responses in tobacco. *Plant Cell* **20**, 1708–1724 (2008).
75. L. C. Boavida, S. McCormick, Temperature as a determinant factor for increased and reproducible in vitro pollen germination in Arabidopsis thaliana. *Plant J.* **52**, 570–582 (2007).
76. M. Dumont *et al.*, A simple protocol for the immunolabelling of Arabidopsis pollen tube membranes and cell wall polymers. *BioProtoc.* **5**, e1502 (2015).
77. H. Wang, L. Jiang, Immunofluorescence labeling of pollen tubes. *BioProtoc.* **4**, e1131 (2014).